TITLE:

Cerebral capillary blood flow upsurge during REM sleep is mediated by A2a receptors

AUTHOR(S):

Tsai, Chia-Jung; Nagata, Takeshi; Liu, Chih-Yao; Suganuma, Takaya; Kanda, Takeshi; Miyazaki, Takehiro; Liu, Kai; ... Vogt, Kaspar E.; Yanagisawa, Masashi; Hayashi, Yu

RIGHT:

京都大学学術情報リポジトリ
KURENAI 紅
Kyoto University Research Information Repository

Cell Reports

Cerebral capillary blood flow upsurge during REM sleep is mediated by A2a receptors

Graphical abstract

Highlights

- A method to directly measure capillary CBF across sleep/wake is developed

- Capillary CBF is highest during REM sleep

- Capillary CBF is comparable between active wakefulness and non-REM sleep

- A2aR signaling is crucial for the CBF upsurge during REM sleep
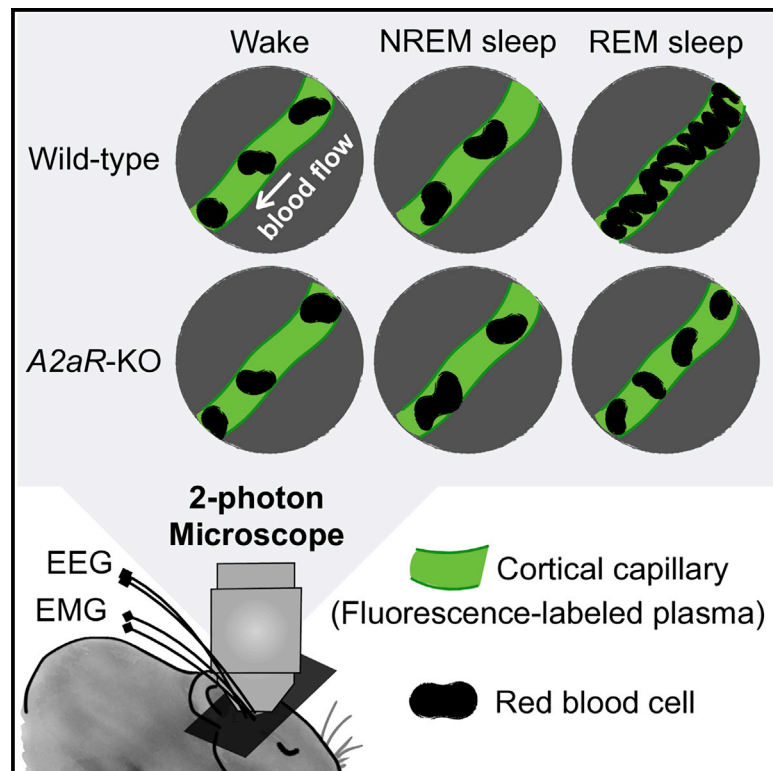
Authors

Chia-Jung Tsai, Takeshi Nagata, Chih-Yao Liu, ..., Kaspar E. Vogt, Masashi Yanagisawa, Yu Hayashi

Correspondence

hayashi.yu.4n@kyoto-u.ac.jp

In brief

Tsai et al. develop a method to directly measure capillary cerebral blood flow (CBF) across the sleep/wake cycle in mice. Capillary CBF is drastically increased during REM sleep, while it is comparable between wakefulness and non-REM sleep. Knocking out the adenosine A2a receptor specifically reduces capillary CBF during REM sleep.

CellPress

京都大学
KYOTO UNIVERSITY

Cell Reports

CellPress
OPEN ACCESS

Article

Cerebral capillary blood flow upsurge during REM sleep is mediated by A2a receptors

Chia-Jung Tsai,[1,8] Takeshi Nagata,[2] Chih-Yao Liu,[1] Takaya Suganuma,[1] Takeshi Kanda,[1] Takehiro Miyazaki,[1] Kai Liu,[3] Tsuyoshi Saitoh,[1] Hiroshi Nagase,[1] Michael Lazarus,[1,2] Kaspar E. Vogt,[1,2] Masashi Yanagisawa,[1,2,4,5,6] and Yu Hayashi[1,2,7,9,*]

[1]International Institute for Integrative Sleep Medicine (WPI-IIIS), University of Tsukuba, Tsukuba, Ibaraki 305-8575, Japan
[2]PhD Program in Human Biology, School of Integrative and Global Majors, University of Tsukuba, Tsukuba, Ibaraki 305-8575, Japan
[3]Center for Mathematical Sciences, Huazhong University of Science and Technology, Wuhan, Hubei 430074, China
[4]Department of Molecular Genetics, University of Texas Southwestern Medical Center, Dallas, TX 75390, USA
[5]Life Science Center for Survival Dynamics (TARA), University of Tsukuba, Tsukuba, Ibaraki 305-8577, Japan
[6]R&D Center for Frontiers of Mirai in Policy and Technology (F-MIRAI), University of Tsukuba, Tsukuba, Ibaraki 305-8575, Japan
[7]Department of Human Health Sciences, Graduate School of Medicine, Kyoto University, 53 Kawahara-cho, Shogoin, Sakyo-ku, Kyoto 603-8363, Japan
[8]Japan Society for the Promotion of Science (JSPS) International Research Fellow, Tokyo 102-0083, Japan
[9]Lead contact
*Correspondence: hayashi.yu.4n@kyoto-u.ac.jp
https://doi.org/10.1016/j.celrep.2021.109558

SUMMARY

Sleep is generally viewed as a period of recovery, but how the supply of cerebral blood flow (CBF) changes across sleep/wake states has remained unclear. Here, we directly observe red blood cells (RBCs) within capillaries, where the actual substance exchange between the blood and neurons/glia occurs, by two-photon microscopy. Across multiple cortical areas, average capillary CBF is largely increased during rapid eye movement (REM) sleep, whereas it does not differ between periods of active wakefulness and non-REM sleep. Capillary RBC flow during REM sleep is further elevated following REM sleep deprivation, suggesting that capillary CBF reflects REM sleep pressure. At the molecular level, signaling via adenosine A2a receptors is crucial; in A2a-KO mice, capillary CBF upsurge during REM sleep is dampened, and effects of REM sleep pressure are abolished. These results provide evidence regarding the dynamics of capillary CBF across sleep/wake states and insights to the underlying mechanisms.

INTRODUCTION

Mammalian sleep comprises two distinct states, non-rapid eye movement (NREM) sleep and rapid eye movement (REM) sleep. Accumulating evidence supports causal roles of both NREM sleep (Chauvette et al., 2012; Miyamoto et al., 2016; Norimoto et al., 2018; Rasch et al., 2007; Roux et al., 2017; Yang et al., 2014) and REM sleep (Boyce et al., 2016; Dumoulin Bridi et al., 2015; Li et al., 2017) in memory consolidation and synaptic plasticity. In addition, biological changes that occur during NREM sleep support critical roles of this sleep stage in basic functions related to brain maintenance or metabolism, such as increased growth hormone secretion (Gronfier et al., 1996; Takahashi et al., 1968), suppressed cortisol secretion (Gronfier et al., 1997), and activation of the glymphatic system (Xie et al., 2013). In contrast, much less is known about how REM sleep may contribute to such basic vital functions.

Cerebral blood flow (CBF) is critical for maintaining energy-dependent processes and clearance of metabolic by-products generated by neuronal activity. Impaired CBF regulation can affect numerous biological functions, and CBF dysregulation correlates with the progression of neurodegenerative disorders such as Alzheimer disease (Hossmann, 1994; Kisler et al., 2017). CBF is strictly regulated and independent of the peripheral circulation (Grant et al., 2005). Until now, various approaches have been used to investigate CBF dynamics across sleep/wake cycles, including positron emission tomography (PET), ultrasound Doppler methods, near-infrared spectroscopy (NIRS), and functional magnetic resonance imaging (fMRI). The conclusions drawn from these different approaches, however, are conflicting. According to studies using $H_2^{15}O$-PET or NIRS, CBF decreases during NREM sleep and is either comparable to or slightly lower than the awake level during REM sleep (Braun et al., 1997; Kubota et al., 2011). In contrast, studies using ultrasonic methods or laser Doppler flowmetry suggest that CBF is highest during REM sleep (Bergel et al., 2018; Grant et al., 2005; Natsubori et al., 2020). In fMRI studies, blood oxygen level-dependent signals, which correlate with increased blood flow, during REM sleep have not yet been strictly compared with other stages, whereas during NREM sleep, they become higher as sleep becomes deeper compared with the awake state (McAvoy et al., 2019). These conflicting findings are likely due to differences in the data processing and normalization procedures used as well as differences in the type of blood vessels that were observed. In addition, some of
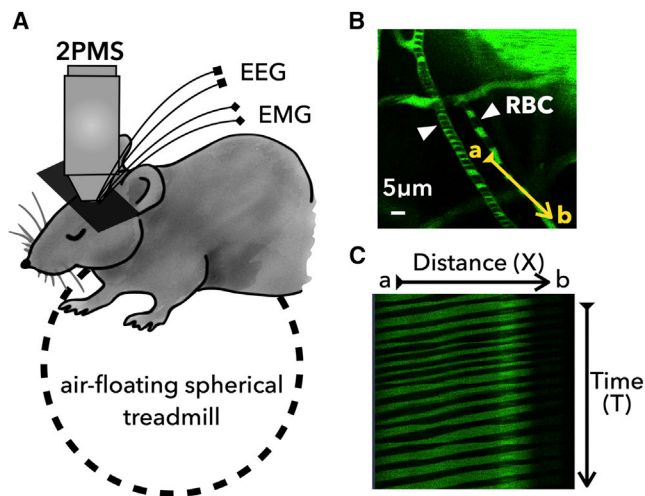
Figure 1. Experimental method for measuring capillary CBF across sleep/wake states in mice

(A) Schematic illustration of the setup for simultaneous 2PM and EEG/EMG recording in mice. Mice were trained to sleep on an air-floating spherical treadmill with their head fixed by a head plate, and imaging was performed through a chronic cranial window.

(B and C) Representative images of the cortical vasculature visualized by labeling blood plasma with FITC-dextran (green). Note that RBCs are not labeled and thus appear black (arrowheads). The movement of RBCs was recorded by repeated single-line scans obtained in the longitudinal direction along the capillary from point a to b (yellow arrow). Line scans (C) obtained in (B) were used to generate a distance-time line scan (XT line scan) image. In this example, the direction of the capillary blood flow is from b to a. From the XT line scan image, RBC velocity and RBC flow were calculated.

the above methods measure a combined effect of CBF and metabolic rates, making interpretation even more difficult, as the cerebral metabolic rate also changes along the sleep/wake cycle, with levels being comparable between wakefulness and REM sleep and lower during NREM sleep, as revealed by ^{18}F-fluoro-2-deoxy-D-glucose PET studies (Maquet et al., 1990). Therefore, the aim of this study was to directly observe the changes in red blood cell (RBC) velocity and flow within cerebral capillaries using two-photon microscopy (2PM) while simultaneously monitoring sleep/wake states.

RESULTS

Capillary CBF largely increased during REM sleep, but was comparable between active wakefulness and NREM sleep

To analyze the dynamics of capillary CBF in unanesthetized mice, we used 2PM to directly measure the movement of individual RBCs within capillaries (Figures 1A and 1B). Sleep stages were simultaneously monitored by recording electroencephalograms (EEGs) and electromyograms (EMGs) (Figure S1A). Capillaries in the cerebral cortex, typically between 30 and 50 μm from the surface of the brain, were targeted for observation. Capillaries in deeper areas were avoided as fluorescent signals derived from the dye had faded by the time the animals started to engage in REM sleep (~3 h after injecting the dye;

Figure S1F). Line scans acquired in the longitudinal direction of the capillary allowed for the detection of temporal changes in the positions of individual RBCs (Figures 1B, 1C, and S1B–S1E). Evaluation of capillary CBF in the parietal cortex, primary somatosensory cortex, and secondary visual cortex during active wakefulness, NREM sleep, and REM sleep revealed significantly increased capillary CBF in all cortical areas during REM sleep in terms of both the RBC velocity (micrometers per millisecond) and flow (number of RBC passing through a defined point; 1 RBC/ms) compared with the other stages (Figures 2A–2C). By contrast, surprisingly, there were no significant differences in the RBC velocity or flow between active wakefulness and NREM sleep. Considering the variability in basal flow among capillaries, we also compared the RBC velocity and flow of each stage normalized to the awake level in each capillary, and the results also showed a similar surge in capillary CBF during REM sleep in all cortical areas (Figures S2A–S2C). The sleep/wake stages did not significantly affect capillary diameter (Figure 2F) or the ratio of RBC flow to velocity (Figure S2F). Thus, the increased capillary CBF during REM sleep is likely not due to the dilation of individual capillaries, but rather to changes in the pre-capillary arteries or structures farther upstream. We observed that, upon entering REM sleep, capillary CBF gradually increased across a period of ~30–50 s and was maintained at a high level thereafter, with some fluctuation until the termination of REM sleep, after which it gradually decreased (Figures 2G–2K and S2M). Thus, in contrast to EEGs and EMGs, which show rapid changes during transitions into or out of REM sleep, capillary blood flow may be regulated by slower mechanisms. Considering that there are also some fluctuations in the EEG during each sleep/wake stage, we next investigated the correlation between capillary CBF and EEG power. RBC velocity was significantly and positively correlated with theta and gamma power during REM sleep (Figure 3B), but not during active wakefulness (Figure 3A). RBC flow was significantly and positively correlated with theta-peak frequency during REM sleep, but not during active wakefulness (Figure 3D). During NREM sleep, RBC velocity was significantly and positively correlated with delta power (Figure 3C). In addition, REM sleep is accompanied by a characteristic dynamism in the theta-gamma coupling (Bandarabadi et al., 2019). However, we did not detect a significant correlation between RBC velocity or flow and theta-gamma coupling during REM sleep (Figure S2L).

Capillary RBC flow was elevated further during rebound REM sleep

We next investigated whether capillary CBF during REM sleep is affected by preceding homeostatic REM sleep pressure. We used the flowerpot method, which disrupts sleep and leads to a strong REM sleep rebound (Maloney et al., 1999; Verret et al., 2006). We confirmed that REM sleep was largely increased immediately in mice subjected to this method of sleep disruption (Figures S3A and S3B). During the rebound REM sleep, the increase in capillary CBF was enhanced compared with that during basal REM sleep in terms of increased relative RBC velocity and RBC flow (Figures 2D, 2E, S2D, and S2E), suggesting that the system underlying the increased capillary CBF during REM sleep is at least partly under the control of REM sleep pressure.

Cell Reports
Article

CellPress
OPEN ACCESS
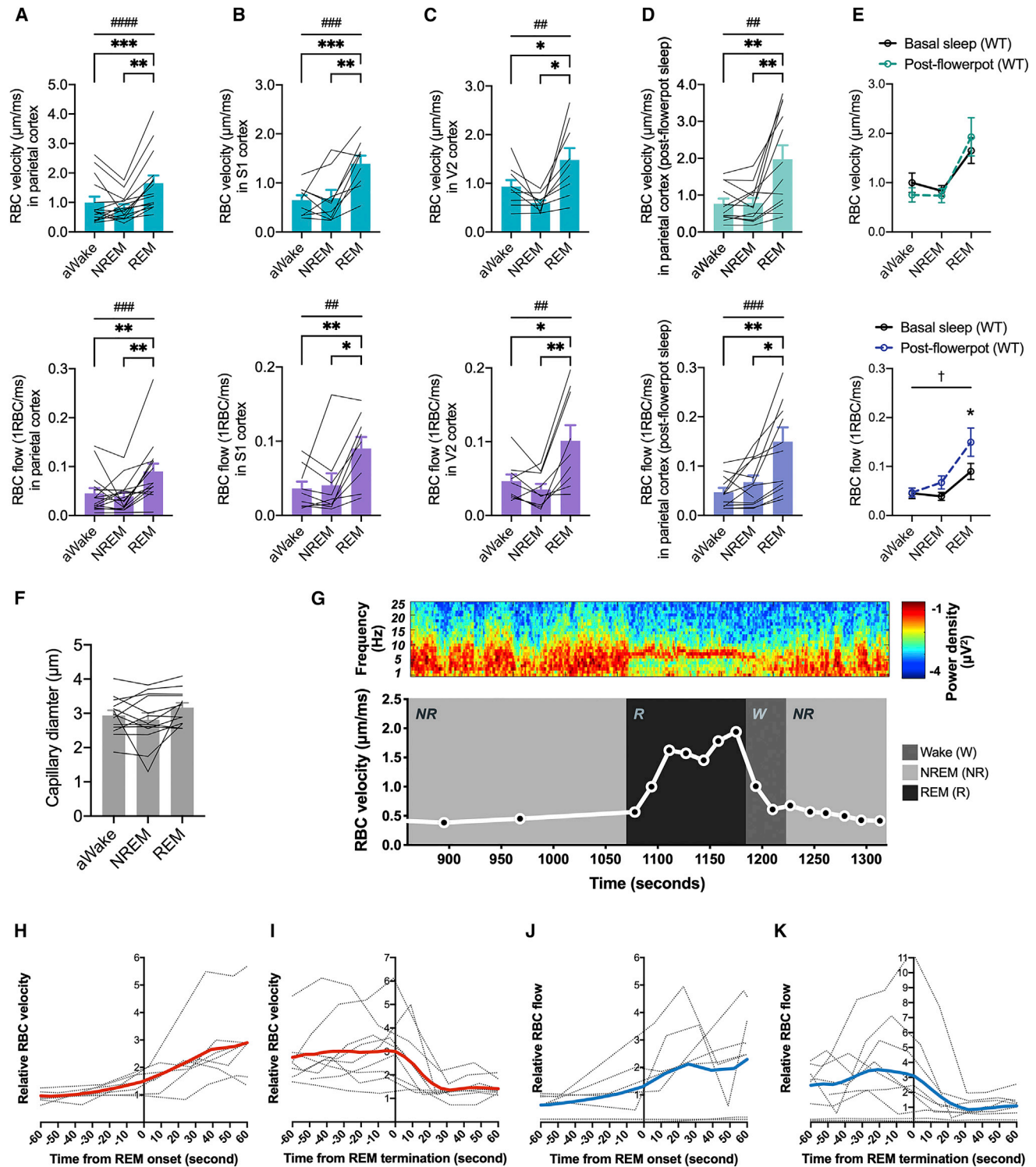
Figure 2. Capillary CBF is largely increased during REM sleep, whereas it is comparable between active wakefulness and NREM sleep

(A–C) RBC velocity and flow (means ± SEMs) during active wakefulness (aWake), NREM sleep (NREM), and REM sleep (REM) in the parietal cortex (A, 6 mice: 2 females and 4 males), primary somatosensory (S1) cortex (B, 3 mice: 1 female and 2 males), and secondary visual (V2) cortex (C, 3 mice: 1 female and 2 males). # indicates a significant effect of the sleep/wake state in repeated-measures 1-way ANOVA (##$p < 0.01$; ###$p < 0.001$; ####$p < 0.0001$). * indicates a significant difference in the post hoc Tukey's multiple comparisons test (*$p < 0.05$; **$p < 0.01$; ***$p < 0.001$) (same in D).

(legend continued on next page)

A2aR is involved in the capillary CBF elevation during REM sleep

We also addressed the molecular mechanism of capillary CBF regulation during sleep. Adenosine is released by neurons and glia and acts as a vasodilator via adenosine A2a receptors (A2aR) (Ngai et al., 2001). In addition, A2aR is a target of caffeine in sleep inhibition, supporting its involvement in sleep regulation, although *A2aR* knockout (*A2aR*-KO) mice exhibit no overt sleep abnormalities or cardiovascular deficits at baseline (Chen et al., 1999; Huang et al., 2005; Tsai et al., 2020). In the *A2aR*-KO mice, capillary CBF in terms of RBC velocity was increased during REM sleep, but to a lesser extent than that in wild-type (WT) mice (Figures 4A, 4B, S2G, and S2H). By contrast, the RBC velocity during active wakefulness or NREM sleep was comparable to WT mice (Figure 4B). In *A2aR*-KO mice, the RBC flow also seemed affected in that RBC flow during REM sleep was not significantly increased compared with that during active wakefulness (Figure 4A). The effect of *A2aR* deletion was more evident when capillary CBF was measured during rebound REM sleep after applying the *A2aR*-KO mice to the flowerpot method. In contrast to WT mice, there was no significant difference in the capillary CBF in terms of both RBC velocity and flow between the basal sleep and the post-flowerpot sleep (Figures 4C, 4D, S2I, and S2J). Moreover, both RBC velocity and flow during the rebound REM sleep were largely decreased in the *A2aR*-KO mice compared to WT mice (Figures 4E and S2K). These results indicate that *A2aR*-KO mice fail to generate the upsurge in capillary CBF during REM sleep, even under high REM sleep pressure.

The general responsiveness of the vasculature in *A2aR*-KO mice was likely unchanged, as suggested by the comparable responses between WT and *A2aR*-KO mice to sodium bicarbonate (NaHCO$_3$), a reagent that increases CBF (Buckley et al., 2013; Yoon et al., 2012) (Figures 5A and 5B). In addition, we confirmed that the duration of REM sleep episodes analyzed in the study was comparable between WT and *A2aR*-KO mice (Figure S3C). Moreover, the EEG power spectrum during REM sleep was not affected (Figure S3E). Thus, reduced capillary CBF during REM sleep in *A2aR*-KO mice is likely not due to a general deterioration of REM sleep episodes. The increase in heart rate during REM sleep (Sakai, 2015) may contribute to the increased capillary CBF. However, the increase in the capillary CBF during REM sleep appeared normal in *A2aR*-KO mice, suggesting that the increase in the capillary CBF can be dissociated from the in-

crease in the heart rate (Figure S3D). Finally, we conducted pharmacological studies to further test the direct involvement of A2aR in regulating capillary CBF. We were not able to test the effects of the A2aR antagonist (ZM241385) because its administration prevented mice from entering sleep (data not shown), which is consistent with a previous report (Halassa et al., 2009). We alternatively tested the effect of A$_{2A}$R PAM-1, which is a positive allosteric modulator of A2aR and thus enhances endogenous A2aR signaling (Korkutata et al., 2019). Administration of A$_{2A}$R PAM-1 to WT mice increased RBC velocity, the effect of which was maximal in REM sleep (Figure 5C). This effect was not observed in the *A2aR*-KO mice, confirming that A$_{2A}$R positive allosteric modulator-1 (PAM-1) affected CBF via A2aR (Figure 5D).

DISCUSSION

By observing the movements of individual RBCs in cerebral capillaries, we were able to directly measure capillary CBF changes across the sleep/wake cycle. Capillary CBF was drastically increased in various cortical areas during REM sleep. This conflicts with findings from human H$_2$^{15}O-PET studies that CBF is highest in many cortical areas during wakefulness (Braun et al., 1997), but is consistent with findings from ultrasound imaging or laser Doppler flowmetry that blood flow is increased in multiple brain areas during REM sleep (Bergel et al., 2018; Natsubori et al., 2020). These differences are likely due to the data processing and normalization procedures used as well as the type of blood vessels that were observed, although differences in animal species may also be involved. The advantage of our method is that it required minimal normalization procedures and detected blood flow from the capillaries, where the actual substance exchange occurs. We also demonstrated that capillary CBF appeared to be the same during active wakefulness and NREM sleep, in contrast to findings using H$_2$^{15}O-PET (Braun et al., 1997), ultrasound Doppler methods (Grant et al., 2005), NIRS (Kubota et al., 2011), or fMRI (McAvoy et al., 2018), and perhaps surprising, considering that the average firing rates of pyramidal cells and metabolic rates are largely decreased during NREM sleep (Evarts, 1964; Maquet et al., 1990).

During transitions to and from REM sleep, we observed a delay in the changes in capillary CBF relative to the changes in cortical EEG activity. Thus, although a change in cortical EEG activity itself

---

(D) RBC velocity and flow (means ± SEMs) in the parietal cortex immediately after subjecting mice to 2 days of sleep disruption using the flowerpot method (4 male mice).

(E) Comparison of RBC velocity and flow (means ± SEMs) in the parietal cortex between basal sleep and sleep after 2 days of sleep disruption induced by the flowerpot method across sleep/wake cycles (same data shown in A and D). † indicates a significant interaction between the condition and sleep/wake state in repeated-measures 2-way ANOVA (†p < 0.05). * indicates a significant difference in the post hoc Sidak's multiple comparisons test (*p < 0.05).

(F) Changes in the capillary diameter (means ± SEMs) across sleep/wake cycles (8 mice: 4 females and 4 males). Data from parietal, S1, and V2 cortices was combined. No significant effect of the sleep/wake state was detected in the repeated-measures 1-way ANOVA.

(G) Representative data showing temporal changes in the EEG power spectrum and the RBC velocity in a capillary during a period containing episodes of NREM sleep (NR), REM sleep (R), and wakefulness (W).

(H–K) Temporal changes in relative RBC velocity (H and I) and flow (J and K) around transitions from NREM sleep to REM sleep (H and J) and REM sleep to wakefulness (I and K).

Of the capillaries analyzed in (A)–(C), those for which measurements around the timing of state transitions were available were plotted. Each gray dotted line represents an individual capillary, and the red or blue line represents the mean value. Each line in (A)–(D) and (F) represents an individual capillary. All of the mice used in this figure were 3.5–4.5 months of age.

Detailed information on statistics is provided in Table S1.

Cell Reports
Article
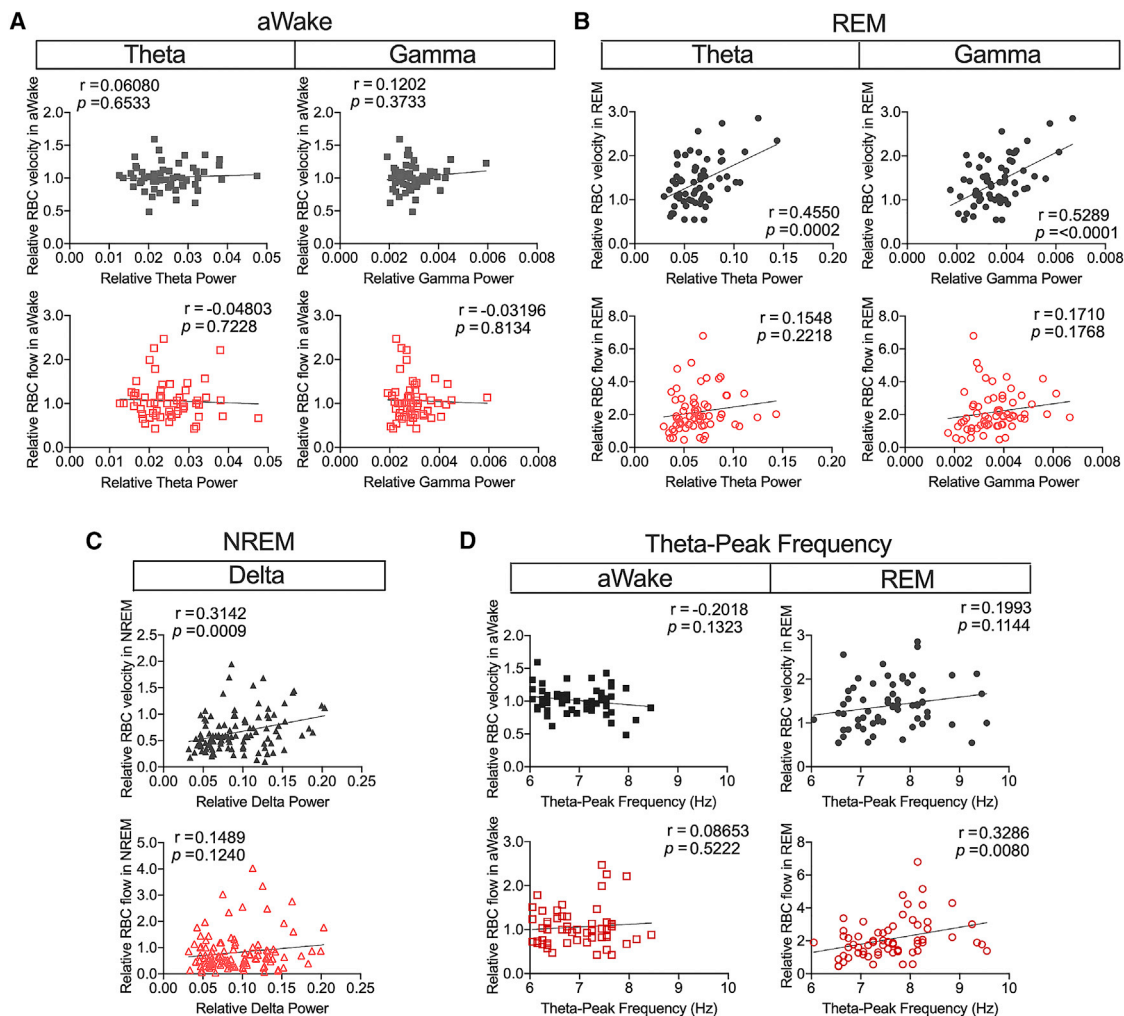
Figure 3. Cortical oscillatory activities are correlated with capillary CBF during REM sleep

(A–C) Correlations between relative RBC velocity (upper panels) or flow (lower panels) and relative theta power (left panels in A and B), relative gamma power (right panels in A and B) or relative delta power (C) during active wakefulness (aWake, A), REM sleep (B), and NREM sleep (C) (3 mice: 2 females and 1 male). Each symbol represents an individual line scan taken during the indicated vigilance state and the horizontal axis indicates the associated EEG power during the 10-s epoch. Pearson correlation coefficient r and level of significance p (2-tailed test) are indicated in each panel (same in D).

(D) Correlations between relative RBC velocity (upper panels) and flow (lower panels) and the theta-peak frequency during aWake (left panels) and REM sleep (right panels) (3 mice: 2 females and 1 male). Each symbol represents an individual line scan taken during the indicated vigilance state, and the horizontal axis indicates the associated theta-peak frequency during the 10-s epoch.

Detailed information on the statistics is provided in Table S1.

should have some effects on CBF via neurovascular coupling, additional mechanisms are likely involved. We demonstrated that A2aR is crucial for the drastic increase in capillary CBF during REM sleep, whereas they are dispensable for maintaining capillary CBF during active wakefulness or NREM sleep. Thus, there is a possibility that adenosine levels in the cerebrum are elevated during REM sleep and cause vasodilation via A2aR. In addition to CBF, REM sleep enhances slow-wave activity in the subsequent NREM sleep episode (Hayashi et al., 2015). Considering that slow-wave activity is also enhanced by adenosine via adenosine 1A receptors (Benington et al., 1995; Bjorness et al., 2009), adenosine signaling may somehow be upregulated during REM sleep. While the average firing rate of pyramidal cells is highest during

wakefulness, pyramidal cells tend to fire in bursts during REM sleep (Evarts, 1964), which may contribute to enhanced adenosine signaling. There is also a possibility that A2aR is functioning in other areas. A recent study using a genetically encoded adenosine sensor revealed that the level of extracellular adenosine in the mouse basal forebrain is highest during REM sleep (Peng et al., 2020). Considering that the basal forebrain sends many projections to the cortex and is involved in regulating CBF (Hotta et al., 2020), A2aR in this area may somehow function to cause CBF elevation during REM sleep. Although an increased heart rate may be one factor contributing to the increased CBF during REM sleep, A2aR-KO mice exhibited normal heart rates during REM sleep, suggesting that CBF is regulated independently
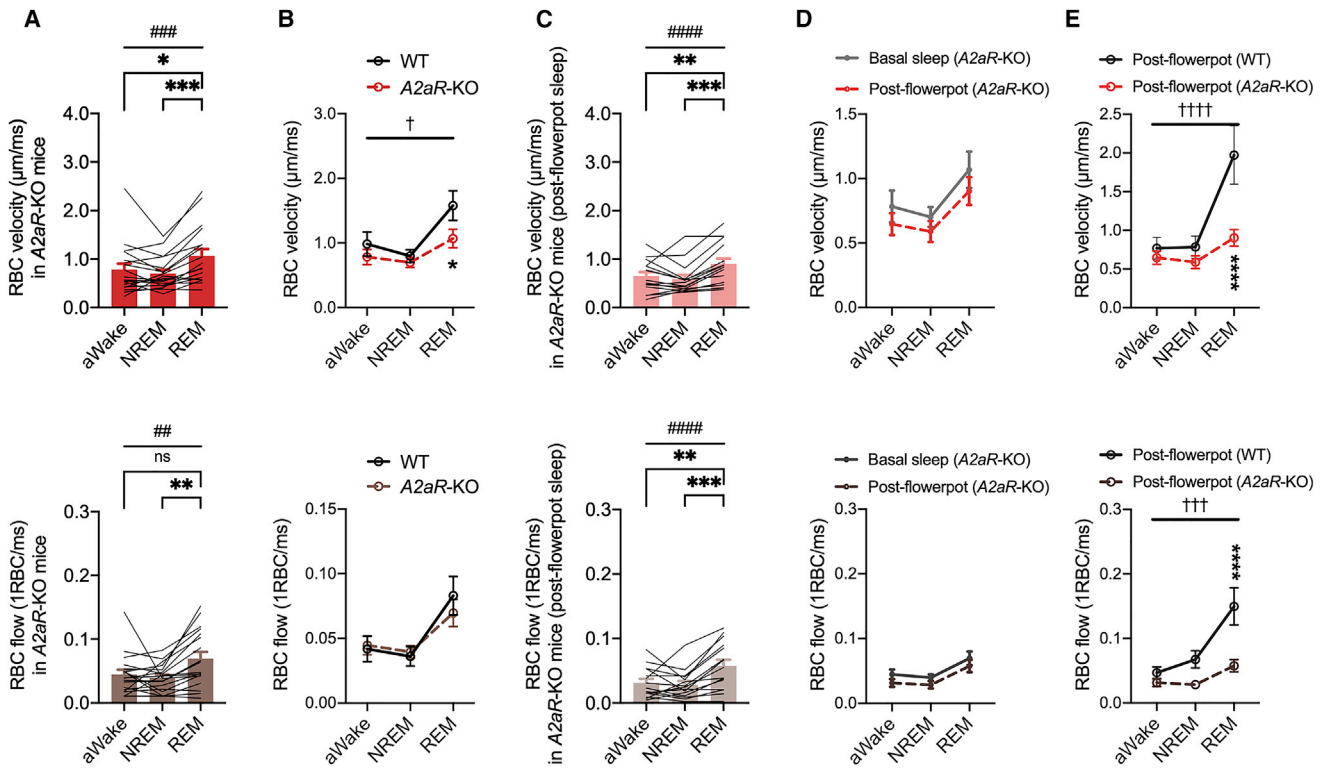
Figure 4. A2aR is involved in the capillary CBF elevation during REM sleep

(A) RBC velocity and flow (means ± SEMs) in the parietal cortex of *A2aR*-KO mice during active wakefulness, NREM sleep, and REM sleep (8 mice: 5 females and 3 males). # indicates a significant effect of the sleep/wake state in repeated-measures 1-way ANOVA (##$p < 0.01$; ###$p < 0.001$). * indicates a significant difference in the post hoc Tukey's multiple comparisons test (*$p < 0.05$; **$p < 0.01$; ***$p < 0.001$).

(B) Comparisons of RBC velocity and flow (means ± SEMs) between WT and *A2aR*-KO mice in the parietal cortex across the sleep/wake cycle (same data shown in Figures 2A and 4A). † indicates a significant interaction between genotype and the sleep/wake state in repeated-measures 2-way ANOVA (†$p < 0.05$). * indicates a significant difference in post hoc Sidak's multiple comparisons test (*$p < 0.05$).

(C) RBC velocity and flow (means ± SEMs) in the parietal cortex immediately after subjecting *A2aR*-KO mice to 2 days of sleep disruption using the flowerpot method (4 mice: 3 females and 1 male). # indicates a significant effect of the sleep/wake state in repeated-measures 1-way ANOVA (####$p < 0.0001$). * indicates a significant difference in the post hoc Tukey's multiple comparisons test (**$p < 0.01$; ***$p < 0.001$).

(D) Comparison of RBC velocity and flow (means ± SEMs) in the parietal cortex of *A2aR*-KO mice between basal sleep and sleep after 2 days of sleep disruption induced by the flowerpot method across sleep/wake cycles (same data shown in Figures 4A and 4C).

(E) Comparison of RBC velocity and flow (means ± SEMs) in the parietal cortex after 2 days of sleep disruption induced by the flowerpot method across sleep/wake cycles between WT and *A2aR*-KO mice (same data shown in Figures 2D and 4C). † indicates a significant interaction between genotype and the sleep/wake state in repeated-measures 2-way ANOVA (†††$p < 0.001$; ††††$p < 0.0001$). * indicates a significant difference in post hoc Sidak's multiple comparisons test (****$p < 0.0001$).

Detailed information on statistics is provided in Table S1.

from the peripheral blood flow. In addition to adenosine, increased acetylcholine and melanin-concentrating hormone (MCH) and decreased noradrenaline, serotonin, orexin, and histamine during REM sleep (Monti, 2013) may also contribute to the increase in CBF. We also found that during REM sleep, but not during wakefulness, there is a positive correlation between RBC velocity or flow and EEG theta and gamma power or EEG theta-peak frequency, which may suggest that cortical oscillatory activities and CBF during REM sleep are affected by a common regulatory system. During NREM sleep, the RBC velocity was positively correlated with delta power, which is consistent with the results of a human PET study (Hofle et al., 1997).

Another advantage of our approach was that we could detect changes in both RBC velocity and flow. RBC flow is determined by RBC velocity and density, which can be differently regulated

under some circumstances (Chaigneau et al., 2003). For example, our study suggested that REM sleep pressure enhances the RBC flow more than the velocity, suggesting that the RBC density was upregulated under such conditions. Further studies are needed to address the molecular mechanism underlying the respective actions of REM sleep on RBC velocity and density. By contrast, a limitation of our current approach was the low throughput. In our study, it was not possible to image the CBF on a large number of capillaries because the fluorescein isothiocyanate (FITC)-dextran was short-lived, lasting only a few hours, whereas it took several hours for the mouse to enter REM sleep following intravenous injection and installation to the 2PM apparatus, making it possible to image only a few capillaries per day.

The increased capillary CBF detected in our study may be important for ensuring an adequate exchange of substances
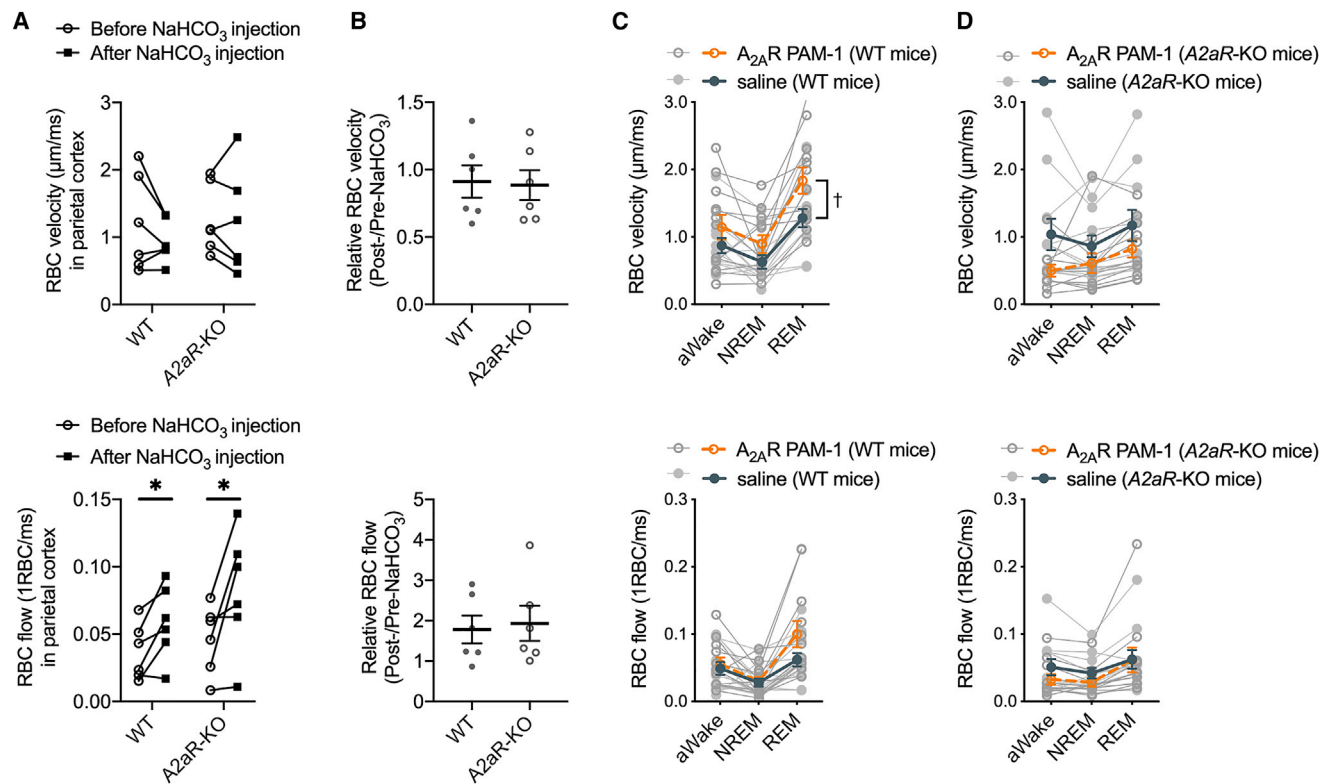
Figure 5. Pharmacological stimulation of A2aR affects capillary CBF

(A and B) Effects of $NaHCO_3$ administration on capillary CBF in the parietal cortex in WT and *A2aR*-KO mice. CBF of each capillary before and after $NaHCO_3$ administration was compared (WT: 2 mice [1 female and 1 male]; *A2aR*-KO: 2 female mice). Comparisons of absolute RBC velocity and flow are shown in (A). * indicates a significant difference in paired t test (*$p < 0.05$). For a comparison of relative RBC velocity and flow (means ± SEMs) in post-$NaHCO_3$ treatment over pre-$NaHCO_3$ treatment (B), no significant difference was detected between genotypes (Welch's test).

(C and D) Effects of $A_{2A}R$ PAM-1 administration on capillary CBF in the parietal cortex of WT mice (C) ($A_{2A}R$ PAM-1: 3 male mice; saline: 3 male mice) and *A2aR*-KO mice (D) ($A_{2A}R$ PAM-1: 3 mice [2 females and 1 male]; saline: 3 mice [2 females and 1 male]). Comparisons of absolute RBC velocity and flow (means ± SEMs) across sleep/wake cycles between conditions are shown in (C) and (D). † indicates a significant main effect of drug in repeated-measures 2-way ANOVA (†$p < 0.05$). Each open/closed circle in (B)–(D), and each line in (C) and (D) represents an individual capillary. All of the mice used in this figure were 3.5–4.5 months of age, except for (A) and (B), in which mice of 7–8 months of age were used.

Detailed information on statistics is provided in Table S1.

---

between the brain and the blood. A reduction in both REM sleep amount and CBF precede dementia, including Alzheimer disease (Pase et al., 2017; Sweeney et al., 2018). Our approach of observing capillary CBF while simultaneously performing EEG/EMG recordings is expected to be effective for future studies elucidating the functional significance of the capillary CBF upsurge during REM sleep.

STAR★METHODS

Detailed methods are provided in the online version of this paper and include the following:

- ● KEY RESOURCES TABLE
- ● RESOURCE AVAILABILITY
  - ○ Lead contact
  - ○ Materials availability
  - ○ Data and code availability
- ● EXPERIMENTAL MODEL AND SUBJECT DETAILS
  - ○ Animals
- ● METHOD DETAILS
  - ○ Study design
  - ○ Animal surgery for chronic two-photon imaging
  - ○ *In vivo* two-photon microscopy
  - ○ EEG/EMG recording under 2PM
  - ○ Sleep stages analysis
  - ○ Analysis of XT line scan images
  - ○ Correlation analysis of capillary CBF and EEG
  - ○ Flowerpot method
  - ○ $NaHCO_3$ and $A_{2A}R$ PAM-1 administration
  - ○ EEG/EMG recording in freely moving mice
- ● QUANTIFICATION AND STATISTICAL ANALYSIS
  - ○ Statistical analysis

SUPPLEMENTAL INFORMATION

Supplemental information can be found online at https://doi.org/10.1016/j.celrep.2021.109558.

CellPress
OPEN ACCESS

Cell Reports
Article

AUTHOR CONTRIBUTIONS

Conceptualization, C.-J.T. and Y.H.; investigation, C.-J.T., C.-Y.L., and T. Suganuma; software, C.-J.T., T.N., and K.L.; formal analysis, C.-J.T., C.-Y.L, and T. Suganuma; resources, T.K., T.M., K.E.V., and M.Y. (for the experimental platform for simultaneous 2PM and EEG/EMG recording) and T. Saitoh, H.N., and M.L. (for synthetized and provided A$_{2A}$R PAM-1); writing – original draft, C.-J.T. and Y.H.; writing – review & editing, C.-J.T. and Y.H.; supervision, Y.H., K.E.V., and M.Y.

DECLARATION OF INTERESTS

The authors declare no competing interests. T.N. is an employee of Mizuho Research & Technologies. T. Suganuma is an employee of Kao Corporation.

INCLUSION AND DIVERSITY

We worked to ensure sex balance in the selection of non-human subjects.

REFERENCES

Bandarabadi, M., Boyce, R., Gutierrez Herrera, C., Bassetti, C.L., Williams, S., Schindler, K., and Adamantidis, A. (2019). Dynamic modulation of theta-gamma coupling during rapid eye movement sleep. Sleep (Basel) *42*, zsz182.

Benington, J.H., Kodali, S.K., and Heller, H.C. (1995). Stimulation of A1 adenosine receptors mimics the electroencephalographic effects of sleep deprivation. Brain Res. *692*, 79–85.

Bergel, A., Deffieux, T., Demené, C., Tanter, M., and Cohen, I. (2018). Local hippocampal fast gamma rhythms precede brain-wide hyperemic patterns during spontaneous rodent REM sleep. Nat. Commun. *9*, 5364.

Bjorness, T.E., Kelly, C.L., Gao, T., Poffenberger, V., and Greene, R.W. (2009). Control and function of the homeostatic sleep response by adenosine A1 receptors. J. Neurosci. *29*, 1267–1276.

Boyce, R., Glasgow, S.D., Williams, S., and Adamantidis, A. (2016). Causal evidence for the role of REM sleep theta rhythm in contextual memory consolidation. Science *352*, 812–816.

Braun, A.R., Balkin, T.J., Wesenten, N.J., Carson, R.E., Varga, M., Baldwin, P., Selbie, S., Belenky, G., and Herscovitch, P. (1997). Regional cerebral blood flow throughout the sleep-wake cycle. An H2(15)O PET study. Brain *120*, 1173–1197.

Buckley, E.M., Naim, M.Y., Lynch, J.M., Goff, D.A., Schwab, P.J., Diaz, L.K., Nicolson, S.C., Montenegro, L.M., Lavin, N.A., Durduran, T., et al. (2013). Sodium bicarbonate causes dose-dependent increases in cerebral blood flow in infants and children with single-ventricle physiology. Pediatr. Res. *73*, 668–673.

Chaigneau, E., Oheim, M., Audinat, E., and Charpak, S. (2003). Two-photon imaging of capillary blood flow in olfactory bulb glomeruli. Proc. Natl. Acad. Sci. USA *100*, 13081–13086.

Chauvette, S., Seigneur, J., and Timofeev, I. (2012). Sleep oscillations in the thalamocortical system induce long-term neuronal plasticity. Neuron *75*, 1105–1113.

Chen, J.F., Huang, Z., Ma, J., Zhu, J., Moratalla, R., Standaert, D., Moskowitz, M.A., Fink, J.S., and Schwarzschild, M.A. (1999). A(2A) adenosine receptor deficiency attenuates brain injury induced by transient focal ischemia in mice. J. Neurosci. *19*, 9192–9200.

Dumoulin Bridi, M.C., Aton, S.J., Seibt, J., Renouard, L., Coleman, T., and Frank, M.G. (2015). Rapid eye movement sleep promotes cortical plasticity in the developing brain. Sci. Adv. *1*, e1500105–e1500109.

Evarts, E.V. (1964). Temporal patterns of discharge of pyramidal tract neurons during sleep and waking in the monkey. J. Neurophysiol. *27*, 152–171.

Grant, D.A., Franzini, C., Wild, J., Eede, K.J., and Walker, A.M. (2005). Autoregulation of the cerebral circulation during sleep in newborn lambs. J. Physiol. *564*, 923–930.

Gronfier, C., Luthringer, R., Follenius, M., Schaltenbrand, N., Macher, J.P., Muzet, A., and Brandenberger, G. (1996). A quantitative evaluation of the relationships between growth hormone secretion and delta wave electroencephalographic activity during normal sleep and after enrichment in delta waves. Sleep *19*, 817–824.

Gronfier, C., Luthringer, R., Follenius, M., Schaltenbrand, N., Macher, J.P., Muzet, A., and Brandenberger, G. (1997). Temporal relationships between pulsatile cortisol secretion and electroencephalographic activity during sleep in man. Electroencephalogr. Clin. Neurophysiol. *103*, 405–408.

Halassa, M.M., Florian, C., Fellin, T., Munoz, J.R., Lee, S.-Y., Abel, T., Haydon, P.G., and Frank, M.G. (2009). Astrocytic modulation of sleep homeostasis and cognitive consequences of sleep loss. Neuron *61*, 213–219.

Hayashi, Y., Kashiwagi, M., Yasuda, K., Ando, R., Kanuka, M., Sakai, K., and Itohara, S. (2015). Cells of a common developmental origin regulate REM/non-REM sleep and wakefulness in mice. Science *350*, 957–961.

Hofle, N., Paus, T., Reutens, D., Fiset, P., Gotman, J., Evans, A.C., and Jones, B.E. (1997). Regional cerebral blood flow changes as a function of delta and spindle activity during slow wave sleep in humans. J. Neurosci. *17*, 4800–4808.

Holtmaat, A., Bonhoeffer, T., Chow, D.K., Chuckowree, J., De Paola, V., Hofer, S.B., Hübener, M., Keck, T., Knott, G., Lee, W.-C.A., et al. (2009). Long-term, high-resolution imaging in the mouse neocortex through a chronic cranial window. Nat. Protoc. *4*, 1128–1144.

Hossmann, K.A. (1994). Viability thresholds and the penumbra of focal ischemia. Ann. Neurol. *36*, 557–565.

Hotta, H., Suzuki, H., Inoue, T., and Stewart, M. (2020). Involvement of the basal nucleus of Meynert on regional cerebral cortical vasodilation associated with masticatory muscle activity in rats. J. Cereb. Blood Flow Metab. *40*, 2416–2428.

Huang, Z.-L., Qu, W.-M., Eguchi, N., Chen, J.-F., Schwarzschild, M.A., Fredholm, B.B., Urade, Y., and Hayaishi, O. (2005). Adenosine A2A, but not A1, receptors mediate the arousal effect of caffeine. Nat. Neurosci. *8*, 858–859.

Kisler, K., Nelson, A.R., Montagne, A., and Zlokovic, B.V. (2017). Cerebral blood flow regulation and neurovascular dysfunction in Alzheimer disease. Nat. Rev. Neurosci. *18*, 419–434.

Korkutata, M., Saitoh, T., Cherasse, Y., Ioka, S., Duo, F., Qin, R., Murakoshi, N., Fujii, S., Zhou, X., Sugiyama, F., et al. (2019). Enhancing endogenous adenosine A$_{2A}$ receptor signaling induces slow-wave sleep without affecting body temperature and cardiovascular function. Neuropharmacology *144*, 122–132.

Kubota, Y., Takasu, N.N., Horita, S., Kondo, M., Shimizu, M., Okada, T., Wakamura, T., and Toichi, M. (2011). Dorsolateral prefrontal cortical oxygenation during REM sleep in humans. Brain Res. *1389*, 83–92.

Li, W., Ma, L., Yang, G., and Gan, W.-B. (2017). REM sleep selectively prunes and maintains new synapses in development and learning. Nat. Neurosci. *20*, 427–437.

Cell Reports
Article

Maloney, K.J., Mainville, L., and Jones, B.E. (1999). Differential c-Fos expression in cholinergic, monoaminergic, and GABAergic cell groups of the ponto-mesencephalic tegmentum after paradoxical sleep deprivation and recovery. J. Neurosci. 19, 3057–3072.

Maquet, P., Dive, D., Salmon, E., Sadzot, B., Franco, G., Poirrier, R., von Frenckell, R., and Franck, G. (1990). Cerebral glucose utilization during sleep-wake cycle in man determined by positron emission tomography and [18F]2-fluoro-2-deoxy-D-glucose method. Brain Res. 513, 136–143.

McAvoy, M.P., Tagliazucchi, E., Laufs, H., and Raichle, M.E. (2019). Human non-REM sleep and the mean global BOLD signal. J. Cereb. Blood Flow Metab. 39, 2210–2222.

Miyamoto, D., Hirai, D., Fung, C.C.A., Inutsuka, A., Odagawa, M., Suzuki, T., Boehringer, R., Adaikkan, C., Matsubara, C., Matsuki, N., et al. (2016). Top-down cortical input during NREM sleep consolidates perceptual memory. Science 352, 1315–1318.

Miyazaki, T., Kanda, T., Tsujino, N., Ishii, R., Nakatsuka, D., Kizuka, M., Kasagi, Y., Hino, H., and Yanagisawa, M. (2020). Dynamics of Cortical Local Connectivity during Sleep-Wake States and the Homeostatic Process. Cereb. Cortex 30, 3977–3990.

Monti, J.M. (2013). The neurotransmitters of sleep and wake, a physiological reviews series. Sleep Med. Rev. 17, 313–315.

Natsubori, A., Tsunematsu, T., Karashima, A., Imamura, H., Kabe, N., Trevisiol, A., Hirrlinger, J., Kodama, T., Sanagi, T., Masamoto, K., et al. (2020). Intracellular ATP levels in mouse cortical excitatory neurons varies with sleep-wake states. Commun. Biol. 3, 491-11.

Ngai, A.C., Coyne, E.F., Meno, J.R., West, G.A., and Winn, H.R. (2001). Receptor subtypes mediating adenosine-induced dilation of cerebral arterioles. Am. J. Physiol. Heart Circ. Physiol. 280, H2329–H2335.

Norimoto, H., Makino, K., Gao, M., Shikano, Y., Okamoto, K., Ishikawa, T., Sasaki, T., Hioki, H., Fujisawa, S., and Ikegaya, Y. (2018). Hippocampal ripples down-regulate synapses. Science 359, 1524–1527.

Pase, M.P., Himali, J.J., Grima, N.A., Beiser, A.S., Satizabal, C.L., Aparicio, H.J., Thomas, R.J., Gottlieb, D.J., Auerbach, S.H., and Seshadri, S. (2017). Sleep architecture and the risk of incident dementia in the community. Neurology 89, 1244–1250.

Peng, W., Wu, Z., Song, K., Zhang, S., Li, Y., and Xu, M. (2020). Regulation of sleep homeostasis mediator adenosine by basal forebrain glutamatergic neurons. Science 369, eabb0556.

Rasch, B., Büchel, C., Gais, S., and Born, J. (2007). Odor cues during slow-wave sleep prompt declarative memory consolidation. Science 315, 1426–1429.

Roux, L., Hu, B., Eichler, R., Stark, E., and Buzsáki, G. (2017). Sharp wave ripples during learning stabilize the hippocampal spatial map. Nat. Neurosci. 20, 845–853.

Sakai, K. (2015). Paradoxical (rapid eye movement) sleep-on neurons in the laterodorsal pontine tegmentum in mice. Neuroscience 310, 455–471.

Sweeney, M.D., Kisler, K., Montagne, A., Toga, A.W., and Zlokovic, B.V. (2018). The role of brain vasculature in neurodegenerative disorders. Nat. Neurosci. 21, 1318–1331.

Takahashi, Y., Kipnis, D.M., and Daughaday, W.H. (1968). Growth hormone secretion during sleep. J. Clin. Invest. 47, 2079–2090.

Tran, C.H.T., and Gordon, G.R. (2015). Acute two-photon imaging of the neurovascular unit in the cortex of active mice. Front. Cell. Neurosci. 9, 11.

Tsai, C.-J., Liu, C.-Y., Lazarus, M., and Hayashi, Y. (2020). Sleep architecture of adenosine A2A receptor-deficient mice. Sleep Biol. Rhythms 18, 275–279.

Verret, L., Fort, P., Gervasoni, D., Léger, L., and Luppi, P.-H. (2006). Localization of the neurons active during paradoxical (REM) sleep and projecting to the locus coeruleus noradrenergic neurons in the rat. J. Comp. Neurol. 495, 573–586.

Xie, L., Kang, H., Xu, Q., Chen, M.J., Liao, Y., Thiyagarajan, M., O'Donnell, J., Christensen, D.J., Nicholson, C., Iliff, J.J., et al. (2013). Sleep drives metabolite clearance from the adult brain. Science 342, 373–377.

Yang, G., Lai, C.S.W., Cichon, J., Ma, L., Li, W., and Gan, W.-B. (2014). Sleep promotes branch-specific formation of dendritic spines after learning. Science 344, 1173–1178.

Yoon, S., Zuccarello, M., and Rapoport, R.M. (2012). pCO(2) and pH regulation of cerebral blood flow. Front. Physiol. 3, 365.

STAR★METHODS

KEY RESOURCES TABLE

REAGENT or RESOURCE	SOURCE	IDENTIFIER
Chemicals, peptides, and recombinant proteins		
FITC-dextran	Thermo Fisher Scientific	Cat# D1823
$NaHCO_3$	Wako-Fujifilm	Cat# 199-01351
$A_{2A}R$ PAM-1	Korkutata et al., 2019	N/A
Experimental models: organisms/strains		
Mouse: wild-type: C57BL/6J	Charles River	N/A
Mouse: *A2aR*-KO: *adenosine A2a receptor knockout*:	Chen et al., 1999	N/A
Oligonucleotides		
Genotyping primer: A2aR_WT_R2 5′-AA AGCCTCAGATGGGAGTCCCAGA-3′	This paper	N/A
Genotyping primer: A2aR_KO_Neo F2 5′-ACTGGGCACAACAGACAATCG-3′	This paper	N/A
Genotyping primer: A2aR_KO_Neo_R2 5′- GCTTCAGTGACAACGTCGAGC-3′	This paper	N/A
Genotyping primer: A2aR_WT_F1 5′- AT GGGCTCCTCGGTGTACATCATGGT-3′	This paper	N/A
Software and algorithms		
Clamplex 10.3	Molecular Devices	RRID: SCR_011323; https://www.molecular devices.com/products/axon-patch-clamp-system/acquisition-and-analysis-software/pclamp-software-suite
MATLAB	MathWorks	RRID: SCR_001622; https://www.mathworks.com/products/matlab.html
Sleep Sign (Version 3)	Kissei comtec	RRID: SCR_018200; http://www.sleepsign.com
VitalRecorder2	Kissei comtec	RRID: SCR_018199; https://www.kicnet.co.jp/solutions/biosignal/humans/biosignal-2/vitalrecorder2/
GraphPad Prism (Version 8)	GraphPad	RRID: SCR_002798; https://www.graphpad.com
ZEN	Carl Zeiss	RRID: SCR_018163, SCR_013672; https://www.zeiss.com/microscopy/us/products/microscope-software/zen.html#introduction
Algorithm of XT line scan analysis	This paper; GitHub	https://github.com/hayashi-laboratory/2PLineScan; https://doi.org/10.5281/zenodo.5119238
Algorithm of EEG power calculation for line scans	This paper; GitHub	https://github.com/hayashi-laboratory/2PEEGcalc; https://doi.org/10.5281/zenodo.5119217
Algorithm of EEG power spectrum analysis	This paper; GitHub	https://github.com/hayashi-laboratory/EEGspectrumAnalysis; https://doi.org/10.5281/zenodo.5119241
Bilateral Filtering (Algorithm)	MATLAB Centeral File Exchange	Douglas Lanman (2021). Bilateral Filtering (https://www.mathworks.com/matlabcentral/fileexchange/12191-bilateral-filtering), MATLAB Central File Exchange. Retrieved February 3, 2021.

(Continued on next page)

Continued

REAGENT or RESOURCE	SOURCE	IDENTIFIER
Abfload (Algorithm)	MATLAB Central File Exchange	Harald Hentschke (2021). Abfload (https://www.mathworks.com/matlabcentral/fileexchange/6190-abfload), MATLAB Central File Exchange. Retrieved February 4, 2021.
Customizable Heatmaps (Algorithm)	MATLAB Central File Exchange	Ameya Deoras (2021). Customizable Heatmaps (https://www.mathworks.com/matlabcentral/fileexchange/24253-customizable-heat-maps), MATLAB Central File Exchange. Retrieved February 4, 2021.
Natural-Order Filename Sort (Algorithm)	MATLAB Central File Exchange	Stephen Cobeldick (2021). Natural-Order Filename Sort (https://www.mathworks.com/matlabcentral/fileexchange/47434-natural-order-filename-sort), MATLAB Central File Exchange. Retrieved February 4, 2021.
MYGINPUT (Algorithm)	MATLAB Central File Exchange	Frederic Moisy (2021). MYGINPUT (https://www.mathworks.com/matlabcentral/fileexchange/12770-myginput), MATLAB Central File Exchange. Retrieved February 4, 2021.
Modulation Index (Algorithm, MATLAB)	Bandarabadi et al., 2019	N/A

RESOURCE AVAILABILITY

Lead contact
Further information and requests for resources and reagents should be directed to and will be fulfilled by the lead contact, Yu Hayashi (hayashi.yu.4n@kyoto-u.ac.jp).

Materials availability
This study did not generate new unique reagents.

Data and code availability
Raw data from all figures in the paper were available at Mendeley (Mendeley Data: https://doi.org/10.17632/dm2gp8yyg8.1). The MATLAB-based programs for XT line scan analysis (https://github.com/hayashi-laboratory/2PLineScan; Zenodo: https://doi.org/10.5281/zenodo.5119238) and EEG power calculation for line scans (https://github.com/hayashi-laboratory/2PEEGcalc; Zenodo: https://doi.org/10.5281/zenodo.5119217), and EEG power spectrum analysis (https://github.com/hayashi-laboratory/EEGspectrumAnalysis; Zenodo: https://doi.org/10.5281/zenodo.5119241) generated during this study are available at GitHub. Several tool packages were used in coding the programs in this study: (1) Douglas Lanman (2021). Bilateral Filtering (https://www.mathworks.com/matlabcentral/fileexchange/12191-bilateral-filtering), MATLAB Central File Exchange. Retrieved February 3, 2021. (2) Harald Hentschke (2021). Abfload (https://www.mathworks.com/matlabcentral/fileexchange/6190-abfload), MATLAB Central File Exchange. Retrieved February 4, 2021. (3) Ameya Deoras (2021). Customizable Heatmaps (https://www.mathworks.com/matlabcentral/fileexchange/24253-customizable-heat-maps), MATLAB Central File Exchange. Retrieved February 4, 2021. (4) Stephen Cobeldick (2021). Natural-Order Filename Sort (https://www.mathworks.com/matlabcentral/fileexchange/47434-natural-order-filename-sort), MATLAB Central File Exchange. Retrieved February 4, 2021. (5) Frederic Moisy (2021). MYGINPUT (https://www.mathworks.com/matlabcentral/fileexchange/12770-myginput), MATLAB Central File Exchange. Retrieved February 4, 2021. The MATLAB script for calculating theta-gamma Modulation Index was provided by Mojtaba Bandarabadi and Antoine Adamantidis (Bandarabadi et al., 2019). Any additional information required to reanalyze the data reported in this paper is available from the lead contact upon request.

EXPERIMENTAL MODEL AND SUBJECT DETAILS

Animals
All animal experiments were approved by the Institutional Animal Care and Use Committee of the University of Tsukuba. Mice were maintained under a 12-h light/dark cycle. Food and water were available *ad libitum*. Strains used in this study were in a C57BL/6J background, and the *adenosine A2a receptor* knockout (*A2aR*-KO) mice (Chen et al., 1999) were provided by Jiang-Fan Chen

CellPress
OPEN ACCESS

Cell Reports
Article

(Wenzhou Medical University). Genotyping of mice was performed using the following primers: A2aR_WT_F1 5′-ATGGGCTCC TCGGTGTACATCATGGT-3′; A2aR_WT_R1 5′-AAAGCCTCAGATGGGAGTCCCAGA-3′; A2aR_KO_Neo_F1 5′-ACTGGGCACAACA GACAATCG-3′; A2aR_KO_Neo_R2 5′- GCTTCAGTGACAACGTCGAGC-3′. Animals with randomized sex and matched age were used for 2PM, and animals with matched sex and age were used for EEG/EMG recording under freely moving conditions. All mice were grouped housed (2 to 5 mice per cage) before surgery, and single housed after surgery to avoid damage to the head plates or recording electrodes. The age and sex of animals used is described in the figure legends. Considering that the upsurge of capillary CBF during REM sleep was similarly observed in both male and female mice in the data related to Figures 2A–2C (data not shown), we mixed the data of both sexes in the subsequent results and we did not perform further analyses on the influence (or association) of sex.

METHOD DETAILS

Study design

Experiments were designed to allow comparison of RBC velocity or flow between different sleep/wake states or conditions or genotypes. Mice were excluded from 2PM if the clarity of the imaging window became low. Mice were excluded from sleep recording in freely moving conditions if EEG/EMG signals were poor prior to data acquisition. Capillaries in which RBC failed to be imaged continuously for a sufficient number of line scans during sleep/wake states due to insufficient head fixture etc. were excluded. The sample sizes in our study were based on a previous study (Tran and Gordon, 2015). We did not encounter problems in replicating results on CBF in different mouse individuals of the same genotype throughout the duration of the study across several mouse cohorts. Analyses of line scan data obtained by 2PM were conducted by an experimenter blinded to the sleep/wake stage. Analyses of EEG/EMG data obtained from freely moving animals were conducted by an experimenter blinded to the genotype. Detailed sample sizes, sex distributions, statistical methods, and the results of each group are indicated in each figure and in Table S1.

Animal surgery for chronic two-photon imaging

Chronic cranial windows were made according to a previous report (Holtmaat et al., 2009). Briefly, adult mice (2-3 months old) were anesthetized with isoflurane (3%–5% for induction and 2%–2.5% for maintenance) and placed in a stereotaxic frame (David Kopf Instruments). The core body temperature was maintained at 32-35°C using a heating pad. A dental drill (Emil Lange C1-500-104-001-001-005, 0.5 mm) was used to carefully thin a circular area on the skull (~3 mm in diameter) over the parietal cortex (1.8 mm lateral and 1.8 mm caudal to bregma) and the portion of the skull was then removed using an angle-tipped needle and sharp forceps. A 4 mm-diameter glass coverslip was placed on the dura and sealed with high viscosity cyanoacrylate glue (Konishi Co., Ltd. #30523). Two EEG electrodes (stainless steel screws) were implanted epidurally over the cortex (1.5 mm lateral and 1.0 mm rostral to lambda, on the hemisphere contralateral to the craniotomy) and the cerebellum (6.8 mm caudal to bregma), respectively. EMG electrodes were stainless steel Teflon-coated wires placed bilaterally into the nuchal muscles and fixed with soldered (Taiyo Electric Ind. Co., Ltd; SE-OST16) ends. Finally, a rectangular aluminum head plate was placed on the skull and attached with dental cement (Super-Bond C&B set; Sun Medical).

In vivo two-photon microscopy

For two-photon observation of the brain during sleep/wake states, head-fixed mice were placed on an air-floating ball, the detail of which was reported previously (Miyazaki et al., 2020). Starting at 1 week after surgery, adult mice (3-4 months old) of either sex underwent a habituation procedure for 3 h daily for at least 7 days to facilitate entrance into sleep on the floating ball apparatus. Capillary CBF was observed using an upright two-photon microscope (Axio Examiner Z1 and LSM 780 NLO, Zeiss) operated by ZEN software (Zeiss). Fluorescence was excited at 800 nm using a tunable Ti:Sa laser (Maitai DeepSee, Spectra-Physics). Laser beams were scanned by galvanometric scanners and focused on the cortical capillaries within 30-50 μm of depth from the brain surface through a 20x water-immersion objective lens (W Plan-Apochromat 20x/NA = 1.0, Zeiss). The emitted fluorescence in a range of 500-550 nm from FITC-dextran was detected with a non-descanned GaAsP detector (BiG, Zeiss).

Capillary CBF was observed between Zeitgeber time (ZT) 3 and ZT10 (ZT0 = light on). White noise (70 dB) was continuously applied throughout the recording sessions to prevent mice from waking up by the sounds generated during the scanning. Before placing mice under the two-photon microscope, the blood plasma was labeled with FITC-dextran (70 kDa molecular weight, Thermo Fisher Scientific, D1823) at a dose of 5 mg/kg body weight in saline by intravenous injection into the lateral tail vein. Blood vessels with diameters of 5 μm or less and only a single RBC passing through each point simultaneously were considered capillaries. Immediately after placing the mice on the imaging apparatus, the mice typically stayed completely awake and often ran actively on the treadmill for about 2 h (Figure S1F). EEG/EMG recording was started during this period, during which data for active wakefulness was collected. For each capillary, repetitive single-line scans were conducted typically along a 20-50 μm range 500 times with 1.3-ms intervals per line to record the velocity and flow of RBC in XT line scans. Later, when the mice entered NREM or REM sleep, XT line scans were acquired for the same capillaries. For NREM sleep episodes, the scanning started at least 1 min after the transition to NREM sleep. For REM sleep episodes, the first scan was started immediately following the transition to REM sleep, but the scans obtained during the first 30 s of the REM sleep episodes were excluded from the statistical analysis. For each capillary, XT line scans were obtained in each sleep/wake state typically 5 to 10 times (minimum 4 times), and each scan was separated by an interval of at least 12 s. More

Cell Reports
Article

frequent scanning was avoided to minimize any potential deleterious effects of the laser on blood flow. The focal plane of imaging was re-adjusted when needed, which mostly occurred when the mouse ran actively or when the mouse entered REM sleep. Cerebral cortical areas were determined by referring to the Allan Brain Atlas (http://portal.brain-map.org/). To analyze the changes in the diameter of the capillaries, XT line scans were acquired in the transverse direction of the vessel. During subsequent offline analyses, the vigilance states were confirmed on the basis of the EEG/EMG data. Heart rate during REM sleep was measured by counting the number of heartbeat spikes recorded in the EMG signal.

EEG/EMG recording under 2PM
During the experiments, we monitored EEG and EMG activity. The EEG and EMG signals were amplified and band-pass filtered (EEG: 40,000x, 0.5–500 Hz; EMG: 4000x, 1.5–1000 Hz) using an analog amplifier (MEG-5200, NIHON KOHDEN). A 16-bit analog-to-digital converter (Digidata 1440A, Molecular Devices) digitized both signals at 2000 Hz, and the signals were acquired using Clampex 10.3 (Molecular Devices). To temporally match the EEG/EMG data to the 2PM data, the 2PM scan timing signals were digitized using the same systems.

Sleep stages analysis
EEG signals were subjected to fast Fourier transform and further analysis using a custom-written MATLAB-based algorithm. The vigilance state was classified as REM sleep, NREM sleep, or wakefulness based on absolute delta (0.5-4 Hz) power, theta (6-10 Hz) power to delta power ratio, and the integral of EMG signals. We applied 10 s sliding window epochs. Epochs with high EMG and low delta power were classified as wakefulness. Epochs with high delta power and low EMG were classified as NREM sleep. Epochs with a high theta power to delta power ratio and extremely low EMG were classified as REM sleep. Prolonged periods of wakefulness (lasting more than an hour) during which mice actively ran on the treadmill were classified as active wakefulness.

Analysis of XT line scan images
XT line scan images were binarized to allow for detection of individual RBC. Then, for each binarized image, the RBC velocity (distance/time) and flow (1 RBC/time) were calculated by measuring the mean slope and number of lines, respectively, using custom-written MATLAB-based algorithms. For each capillary, the mean value was calculated from multiple (at least 3) scan images for each vigilance state. The experimenter was blinded to the sleep stage when analyzing all line scan images. Relative RBC velocity and flow were calculated by dividing the average value of each capillary during each vigilance state by the median value of that capillary during active wakefulness.

Correlation analysis of capillary CBF and EEG
For each line scan, absolute RBC velocity and flow were normalized to the median value of the same capillary during active wakefulness. 10 s epochs and 5 s sliding windows were used to calculate EEG power. For each mouse, absolute theta (6-10 Hz), gamma (25-100 Hz) or delta (0.5-4 Hz) power was normalized to the average power (0-30 Hz) across all REM sleep epochs. For each line scan, the theta-peak frequency was assigned to the frequency bin with the highest EEG power between 6 to 10 Hz (0.1 Hz resolution) using 10 s epochs. Modulation Index calculated by a MATLAB script provided by Mojtaba Bandarabadi and Antoine Adamantidis was used to measure theta (6-10 Hz)-gamma (55-95 Hz) coupling (Bandarabadi et al., 2019).

Flowerpot method
The flowerpot method was performed as previously described (Verret et al., 2006). Briefly, a stainless-steel platform (3 cm in diameter and height) was placed in a cage that was filled with water to a depth of 2 cm. Food and water were easily accessible to the mice from the top. Mice were placed in this cage for 23.5 h, starting at ZT4.5. Mice were then given a 30-min rest period in the home cage, during which the flowerpot cage was cleaned. This was repeated for 2 days (for simultaneous 2P measurements and EEG/EMG recording) or 3 days (for EEG/EMG recording only). Similar to other experiments, 2P measurements was performed from ZT5 to ZT8, considering that the REM sleep rebound was very high during this period (Figures S3A and S3B).

NaHCO$_3$ and A$_{2A}$R PAM-1 administration
NaHCO$_3$ (Wako-Fujifilm, 199-01351) was dissolved in distilled water (1M) and administered intraperitoneally (1.7 g/kg body weight). A$_{2A}$R PAM-1 was prepared according to a previous paper (Korkutata et al., 2019), dissolved in saline (7.5 mg/ml), and administered intraperitoneally (75 mg/kg body weight).

EEG/EMG recording in freely moving mice
To confirm the occurrence of REM sleep rebound after subjecting mice to the flowerpot method and to compare the EEG power spectrum between *A2aR*-WT and *A2aR*-KO mice, EEG/EMG signals were obtained from freely moving mice according to a previous study (Hayashi et al., 2015). Briefly, EEG electrodes were implanted epidurally over the parietal cortex and cerebellum, and EMG electrodes were placed bilaterally into the nuchal muscles, similar to that in mice used in the 2PM experiments. The mice were allowed to recover in their home cage for at least 3 weeks and were then habituated to the sleep recording cages for 5 d. The EEG/EMG data were filtered (band pass 0.5-250 Hz), collected, and digitized at a sampling rate of 500 Hz, and further filtered post hoc

by software (EEG: high pass 0.5 Hz). For judging vigilance stages, EEG signals were subjected to fast Fourier transform and further analysis using SleepSign (Kissei Comtec). The vigilance state in each 4 s epoch was manually classified as wakefulness, NREM sleep, or REM sleep according to the same criteria used for the 2PM experiments. If a single epoch contained multiple states, the state with the longest duration was assigned. For EEG power spectrum comparison, a custom-written MATLAB-based algorithm was used. For each individual, the mean EEG power spectrum of REM sleep epochs was calculated and normalized by the total EEG power across all frequencies and across all 24 h. To avoid the effect of mixed states, epochs containing multiple states were excluded.

QUANTIFICATION AND STATISTICAL ANALYSIS

Statistical analysis

All statistical analyses were performed in Prism8 (GraphPad). All bar graphs represent the mean ± s.e.m. of all samples in each group. At least two capillaries per mouse were analyzed in all figures, except for one WT and one *A2aR*-KO mouse from which only one capillary was used in the statistical analysis. Detailed sample sizes, sex distributions, statistical methods, and the results of each group are indicated in each figure and in Table S1. Where applicable, all statistical tests were two-tailed. Statical significance was considered when $p < 0.05$.